14th Deep Sea Offshore Wind R&D Conference, EERA DeepWind'2017, 18-20 January 2017, Trondheim, Norway

OC5 Project Phase II: Validation of Global Loads of the DeepCwind Floating Semisubmersible Wind Turbine

Amy N. Robertson[a]*, Fabian Wendt[a], Jason M. Jonkman[a], Wojciech Popko[b], Habib Dagher[c], Sebastien Gueydon[d], Jacob Qvist[e], Felipe Vittori[f], José Azcona[f], Emre Uzunoglu[g], Carlos Guedes Soares[g], Rob Harries[h], Anders Yde[i], Christos Galinos[i], Koen Hermans[j], Jacobus Bernardus de Vaal[k], Pauline Bozonnet[l], Ludovic Bouy[m], Ilmas Bayati[n], Roger Bergua[o], Josean Galvan[p], Iñigo Mendikoa[p], Carlos Barrera Sanchez[q], Hyunkyoung Shin[r], Sho Oh[s], Climent Molins[t], Yannick Debruyne[u]

[a]National Renewable Energy Laboratory, USA
[b]Fraunhofer IWES, Germany
[c]University of Maine, USA
[d]Maritime Research Institute Netherlands, Netherlands
[e]4Subsea, Norway
[f]CENER, Spain
[g]CENTEC, Portugal
[h]DNV GL, England
[i]Technical University of Denmark, Denmark
[j]European Centre of the Netherlands, The Netherlands
[k]Institute for Energy Technology, Norway
[l]IFP Energies nouvelles, France
[m]PRINCIPIA, France
[n]Politecnico di Milano, Italy
[o]Siemens PLM, Spain
[p]Tecnalia, Spain
[q]Universidad de Cantabria – IH Cantabria, Spain
[r]University of Ulsan, Korea
[s]University of Tokyo, Japan
[t]Universitat Politècnica de Catalunya, Spain
[u]WavEC Offshore Renewables, Portugal

* Corresponding author. Tel.: +1-303-384-7157.
E-mail address: amy.robertson@nrel.gov

Abstract

This paper summarizes the findings from Phase II of the Offshore Code Comparison, Collaboration, Continued, with Correlation project. The project is run under the International Energy Agency Wind Research Task 30, and is focused on validating the tools used for modeling offshore wind systems through the comparison of simulated responses of select system designs to physical test data. Validation activities such as these lead to improvement of offshore wind modeling tools, which will enable the development of more innovative and cost-effective offshore wind designs.

For Phase II of the project, numerical models of the DeepCwind floating semisubmersible wind system were validated using measurement data from a $1/50^{th}$-scale validation campaign performed at the Maritime Research Institute Netherlands offshore wave basin. Validation of the models was performed by comparing the calculated ultimate and fatigue loads for eight different wave-only and combined wind/wave test cases against the measured data, after calibration was performed using free-decay, wind-only, and wave-only tests. The results show a decent estimation of both the ultimate and fatigue loads for the simulated results, but with a fairly consistent underestimation in the tower and upwind mooring line loads that can be attributed to an underestimation of wave-excitation forces outside the linear wave-excitation region, and the presence of broadband frequency excitation in the experimental measurements from wind. Participant results showed varied agreement with the experimental measurements based on the modeling approach used. Modeling attributes that enabled better agreement included: the use of a dynamic mooring model; wave stretching, or some other hydrodynamic modeling approach that excites frequencies outside the linear wave region; nonlinear wave kinematics models; and unsteady aerodynamics models. Also, it was observed that a Morison-only hydrodynamic modeling approach could create excessive pitch excitation and resulting tower loads in some frequency bands.

1. Introduction

Offshore wind turbines are designed and analyzed using comprehensive simulation tools (or codes) that account for the coupled dynamics of the wind inflow, aerodynamics, elasticity, and controls of the turbine, along with the incident waves, sea current, hydrodynamics, mooring dynamics, and foundation dynamics of the support structure. The Offshore Code Comparison Collaboration (OC3) and Offshore Code Comparison Collaboration Continuation (OC4), operated under International Energy Agency Wind Tasks 23 and 30, were established to verify the accuracy of offshore wind turbine modeling tools through code-to-code comparisons. These projects were successful in showing the influence of different modeling approaches on the simulated response of offshore wind systems. Code-to-code comparisons, though, can only identify differences. They do not determine which solution is the most accurate. To address this limitation, an extension of Task 30 was initiated: the Offshore Code Comparison Collaboration, Continued, with Correlation (OC5). This project's objective is validating offshore wind modeling tools through the comparison of simulated responses to physical response data from actual measurements. The project involves three phases using data from both floating and fixed-bottom systems, and from both scaled tank testing and full-scale, open-ocean testing.

Other research projects have or are now also investigating modeling approaches for offshore wind systems, with specific focuses on wind turbine wakes (IEA Task 31) [1], floating offshore wind systems (INNWIND) [2], or extreme wave loading (WaveLoads project) [3]. The OC5 (and OC3 and OC4) projects are unique, however, in how they are run—with a large number of participants from a variety of institutions using different modeling tools, theories, and approaches, with a concentrated effort to understand the drivers of modeling differences when they arise. The project is run collaboratively with members from the wind and offshore industries, as well as universities,

research institutions, and certifying agencies. The work is analyzed collectively, and multiple iterations of the results are computed to better understand the reasons for the differences between participant results, thus allowing for a better understanding of appropriate modeling practices and methods for offshore wind analysis.

In Phase I of the OC5 project, two different data sets were analyzed, both focusing on validation of hydrodynamic loads on cylinders, with no wind turbine present. The data sets used came from wave tank experiments, with Phase Ia examining a suspended, rigid cylinder tested at Marintek [4] and Phase Ib considering a flexible cylinder fixed to a sloped floor [5], tested by the WaveLoads project, which was run by the Technical University of Denmark (DTU) and Danish Hydraulic Institute. Findings from Phase I included the need for the proper choice of hydrodynamic coefficients, higher-order wave theory, complex seabed models, and nonlinear hydrodynamic theory (such as wave stretching and second- and higher-order models) to accurately predict the hydrodynamic loads and response of a structure [4], [5].

Phase II of the project, which is the focus of this paper, builds on this work by examining a more complicated floating offshore wind system with a wind turbine. The system is a floating semisubmersible, tested by the DeepCwind consortium in 2013 at the Maritime Research Institute Netherlands (MARIN) offshore wave basin under combined wind and wave loading. It is similar to the system analyzed within Phase II of OC4 [6], except that the turbine modeled in this project is the one tested in the tank experiment, rather than an idealized model of the National Renewable Energy Laboratory's (NREL's) 5-MW reference wind turbine [7]. OC4 only compared results between simulations, and did not work with test data. By using a similar system, the work done in OC4 can be used to support and advance our understanding of the system within OC5.

Academic and industrial project partners from 11 different countries participated in the task. Those actively involved in Phase II are: NREL (USA), MARIN (Netherlands), 4Subsea (Norway), CENER (Spain), CENTEC (Portugal), DNV GL (United Kingdom), DTU (Denmark), Energy research Centre of the Netherlands (ECN - Netherlands), the Institute for Energy Technology (IFE - Norway), IFP Energies nouvelles (France), PRINCIPIA (France), Politecnico di Milano (PoliMi - Italy), Siemens PLM (Spain), Tecnalia (Spain), Universidad de Cantabria (UC-IHC - Spain), University of Ulsan (UOU - Korea), University of Tokyo (UTokyo - Japan), Universitat Politècnica de Catalunya (UPC - Spain), and Wave Energy Center (WavEC - Portugal).

The remainder of this paper is organized as follows. Section 2 provides a description of the model tests from which the experimental data were obtained, Section 3 covers analysis of that data with a description of some issues that were encountered, Section 4 describes the characteristics and the approach used by participants to model the test system, Section 5 describes the process used to calibrate the simulation models of the test system, and Section 6 covers the validation of simulation results against the test measurements. Finally, the conclusions drawn from this work and suggestions of future work are given in Section 7.

2. Model Test Description

In 2011, the DeepCwind Consortium, led by the University of Maine (UMaine), performed an extensive series of floating wind turbine model tests at the MARIN offshore wave basin [8]. These tests, which were conducted at 1/50th scale, investigated the response of three floating wind turbine concepts subjected to simultaneous wind and wave environments. During these tests, it was found that the geometrically scaled wind turbine did not perform as expected in the low-Reynolds number wind environment. A new turbine was therefore built (the MARIN Stock Wind Turbine) that produced better scaled thrust and torque loads (see [9], [10]). This turbine was
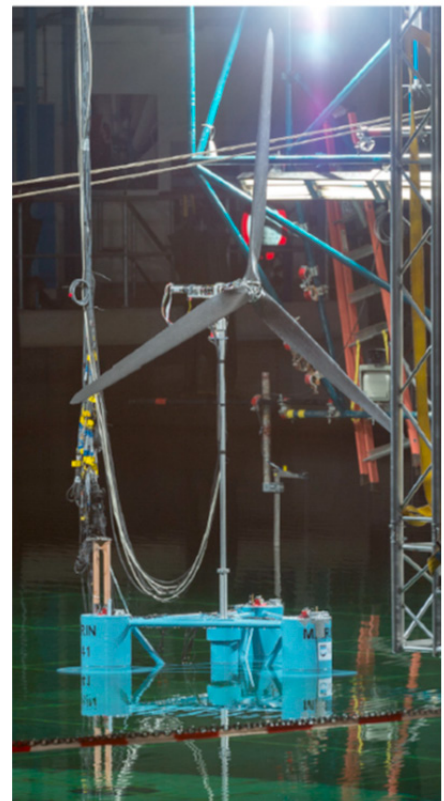

Fig. 1. Instrumented OC5-DeepCwind model in the MARIN offshore basin [11]

mounted on the semisubmersible that was tested in 2011 and retested in 2013. This retest is what was examined in Phase II of the OC5 project.

The turbine is a 1/50th-scale horizontal-axis model of the NREL 5-MW reference wind turbine [7] with a flexible tower affixed atop a semisubmersible (see Fig. 1). The tower was scaled to ensure a match of the first natural bending frequency, but the diameter of the tower was much smaller than it should have been. Therefore, it did not match the level of wind drag for a real system. The system is moored using brass chain in a catenary configuration (without any truncation), with a correctly scaled above and under water weight and stiffness/displacement relationship. No mention was given in the test report [11]

Fig. 2. Layout of the floating wind system in the tank [11]

regarding the appropriate scaling of the chain diameter to ensure a match of the mooring line hydrodynamic excitation and damping.

The system was tested under Froude-scaled wind and wave loads; see [12] for more details on the scaling process. The wind environment in the offshore basin was realized via a wind machine that exhibits negligible swirl and low turbulence intensity in the flow field (on average 5% across the rotor plan). Minimal variation in the average wind speed was seen spatially across the rotor, except for a significant drop at the very bottom edge (see [13] for further information). Recorded data from the floating wind turbine models included rotor torque and position, tower-top and tower-base forces and moments, mooring line tensions, six degrees-of-freedom platform motions, and accelerations at key locations on the nacelle, tower, and platform. A large number of tests were performed, ranging from simple free-decay tests to complex operating conditions with irregular sea states and dynamic winds.

Tables 1−7 provide the relevant properties of the system (center of mass [CM]; still water line [SWL]), including the structural and hydrodynamic properties. Figure 2 shows the layout of the model in the tank, as well as the global motions for surge (x-displacement) and sway (y-displacement). Heave (z-displacement) follows the right-hand rule. Roll, pitch, and yaw rotations are about the x, y, and z axes. More information on the experimental setup can be found in [8] and [13]. All information presented in this paper is given at full scale, but represents the behavior of the model-scale system.

3. Data Analysis

The measurements from the tests were examined prior to use, to determine quality and assess uncertainties. No formal quality checks or uncertainty assessments were performed by those carrying out the testing, but rigorous methods were used to calibrate the instrumentation, ensure repeatability of the wave environment, and create a smooth and spatially consistent (as possible) wind environment with minimal swirl and turbulence. No information was provided on the repeatability of the wave and wind excitation, or the system response, hampering the ability to do a post-test uncertainty assessment. Some insight into the uncertainty of these tests and what should be considered in future test campaigns is provided in [14]. Issues that were discovered during the data analysis include:

- *Tower-top moment:* Measurements were recorded for the forces and moments at both the top and bottom of the tower using a six-axis load cell. The force and moment at the tower bottom showed a consistent
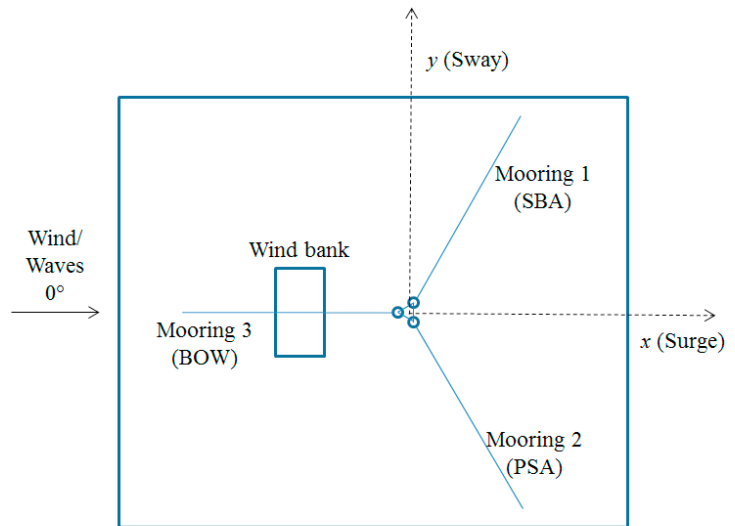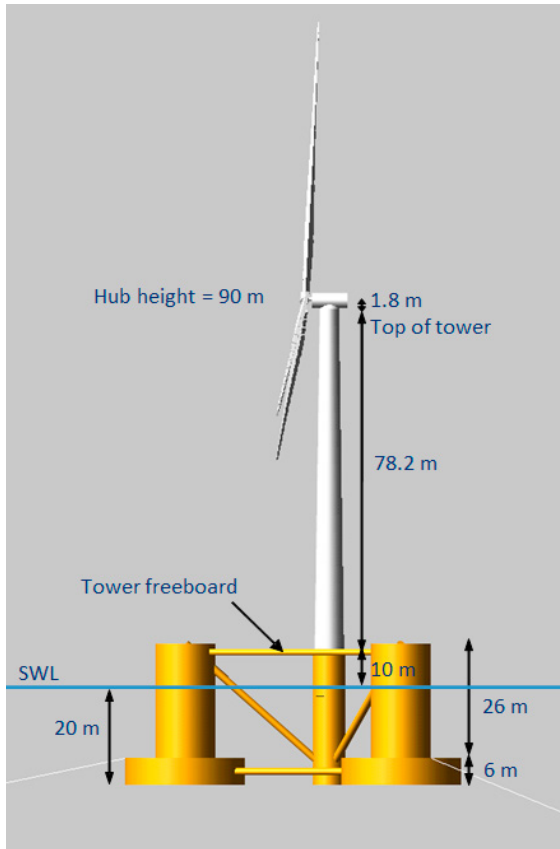
Fig. 3. OC5-DeepCwind floating wind system design

Table 1. Full system structural properties.

Mass	1.3958E+7 kg
Draft	20 m
Displacement	1.3917E+4 m^3
CM location below SWL	8.07 m
Roll inertia about system CM	1.3947E+10 kg-m^2
Pitch inertia about system CM	1.5552E+10 kg-m^2
Yaw inertia about system CM	1.3692E+10 kg-m^2

Table 2. Blade structural properties.

Length (w.r.t. root along axis)	61.5 m
Overall (integrated) mass	2.2333E+4 kg
Second mass moment of inertia (w.r.t. root)	1.48248E+7 kg-m^2
First mass moment of inertia (w.r.t. root)	4.5727E+5 kg-m
CM location (w.r.t. root along axis)	20.475 m

Table 3. Tower properties.

Elevation to tower base above SWL	10 m
Elevation to tower top above SWL	88.2 m
Mass	1.778E+5 kg
Mass including instrumentation	4.935E+5 kg
CM location above SWL	43.85 m

Table 4. Rotor-nacelle-assembly (RNA) structural properties.

Rating	5 MW
Rotor, hub diameter	126 m, 3 m
Hub height (HH)	90 m
Yaw bearing height from SWL	88.2 m
Dist. from yaw bearing to shaft	1.8 m
Overhang, tilt, precone (from HH)	10.6 m, 0°, 0°
Rotor mass (blades only)	6.70E+4 kg
Nacelle mass (including hub)	4.779E+5 kg
Total RNA mass	5.449E+5 kg
CM location of RNA (rel. to HH)	(-1.13 m, 0 m, 0 m)
RNA roll inertia about CM	6.6413E+07 kg-m^2
RNA pitch inertia about CM	8.5004E+07 kg-m^2
RNA yaw inertia about CM	8.5004E+07 kg-m^2

Table 5. Floating platform structural properties.

Mass, including ballast	1.2919E+7kg
CM location below SWL	14.09 m
Roll inertia about CM	7.5534E+9 kg-m^2
Pitch inertia about CM	8.2236E+9 kg-m^2
Paw inertia about CM	1.3612E+10 kg-m^2

Table 6. Floating platform hydrodynamic properties.

Water density	1025 kg/m^3
Water depth	200 m
Displaced water volume	13917 m^3
Center of buoyancy below SWL	13.15 m
Static buoyancy force	1.3989E+8 N
Hydrostatic restoring in heave	3.836E+06 N/m
Hydrostatic restoring in roll about platform centerline at SWL	-3.776E+08 N-m/rad
Hydrostatic restoring in pitch about platform centerline at SWL	-3.776E+08 N-m/rad

Table 7. Mooring system properties.

Number of mooring lines	3
Angle between adjacent lines	120°
Radius to anchors from centerline	837.6 m
Radius to fairleads from centerline	40.868 m
Unstretched mooring line length	835.5 m
Volume-equivalent diameter, line 1	0.1369 m
Volume-equivalent diameter, line 2	0.1398 m
Volume-equivalent diameter, line 3	0.1393 m
Mooring line mass density, line 1	125.6 kg/m
Mooring line mass density, line 2	125.8 kg/m
Mooring line mass density, line 3	125.4 kg/m
Equiv. line extensional stiffness, line 1	7.520E+8 N
Equiv. line extensional stiffness, line 2	7.461E+8 N
Equiv. line extensional stiffness, line 3	7.478E+8 N
Pretension, line 1	1.107E+6 N
Pretension, line 2	1.112E+6 N
Pretension, line 3	1.148E+6 N

relationship, but the tower-top moment had significant variation from the tower-top force measurement. Therefore, it was decided to neglect the tower-top moment measurement, and instead focus on the shear force measurements to assess the loads in the tower.

- *Instrumentation bundle:* A significant amount of wires were used to connect the instruments to the data acquisition system, as can be seen hanging off of the tower in Fig. 1. These wires were attached to the upper half of the tower, and their mass was included in the details of the tower properties. However, during the motion of structure, there is potential that the cable bundle could pull on the tower, acting similar to a mooring line. The influence of these wires was only assessed through a pitch free-decay test, which showed a shift in the pitch natural frequency, but no significant influence on the pitch damping.

- *Surge equilibrium:* The data showed that the equilibrium position of the structure varied between tests. The assumption is that this was caused by the mooring lines being dragged to a new position after tests that have caused large excursions of the horizontal motions. Another possibility is the influence of the instrumentation cable bundle. The equilibrium position prior to testing was recorded for the wave-only tests, but is not known for those tests that included wind. For the wave-only tests, this equilibrium value was subtracted from the results. However, estimates of the drift offset from waves should be considered highly uncertain because of this issue.

- *Wind response:* The tests showed large levels of system response across broad frequency ranges during wind excitation. Several attempts were made to create a wind environment that would generate similar levels of response in the simulation models, but nothing was able to achieve the same levels as the tests (see [13] for more details). Only one measurement of the average spatial variation of the wind speed was provided, with no uncorrupted measurements of the wind during testing or assessment of the spatial coherence, limiting our understanding of the wind field. Also, no results from repeat tests for the wind calibration were available.

4. Modeling Approach

A list of the tools used in this study is provided in Table 8, which also shows the participant using the tool, and the modeling approach employed. These are the characteristics employed in the simulations, and not what attributes are available in the tools; however, some characteristics were turned off for certain load cases, such as regular wave simulations.

The colors shown in the table indicate that a given participant and their associated tool are including the described modeling characteristics for their analysis. The abbreviations that are used in the table are described below, as well as the differentiation between the pink and green coloration.

- *Aerodynamics*
    - o Dyn. Wake = dynamic wake
    - o Unst. Airfoil = unsteady airfoil aerodynamics
- *Hydrodynamics*
    - o 2nd+ WK = second-order (or higher) wave kinematics
    - o 1st PF = first-order potential flow model (green = Morison drag also included via strip theory, pink = viscous drag approximated by a damping matrix)
    - o 2nd PF = second-order potential flow model
    - o ME = Morison equation (pink = full, green = only drag term)
    - o Meas. Wave = measured wave elevation
    - o Stretch = wave stretching
    - o Inst. Pos. = hydrodynamic forces calculated at the instantaneous position of the structure

- *Moorings*
  - Dyn. = dynamic mooring model
  - Hydro Exc. = hydrodynamic loads on the moorings caused by wave excitation
  - Seabed Fric. = seabed friction

Table 8. Summary of participants, tools/codes, and modeling approach used in the validation exercise.

Participant	Code	Aerodyn.		Hydrodynamics							Moorings		
		Dyn. Wake	Unst. Airfoil	2nd + WK	1st PF	2nd PF	ME	Meas. Wave	Stretch	Inst. Pos.	Dyn.	Hydro Exc.	Seabed Fric.
4Subsea	OrcaFlex-FAST v8	●	●				●			●	●	●	●
CENER	FAST v6 + OPASS	●	●		○		●			●	●	●	●
CENTEC	FAST v8	●	●			●	●			●	●	●	●
DNV GL	Bladed 4.8	●	●				●			●	●	●	●
DTU ME	HAWC2	●	●				○			●	●	●	●
DTU PF	HAWC2	●	●		○					●	●	●	●
ECN-MARIN	aNySIM-PHATAS v10	●	●			Diff.-only	●			●	●	●	●
IFE	3DFloat	●					○			●	●	●	●
IFP_PRI	DeepLines Wind V5R2	●	●				●			●	●	●	●
NREL PF	FAST v8	●	●			●	●			●	●	●	●
NREL ME	FAST v8	●	●				○			●	●	●	●
POLIMI	FAST v8.15	●	●	Diff.-only			●			●	●	●	●
Siemens PLM	Samcef Wind Turbines	●	●				○			●	●	●	●
Tecnalia F7O	FAST v7 + OrcaFlex 9.7	●	●		○		●			●	●	●	●
Tecnalia F8	FAST v8.16	●	●			●	●			●	●	●	●
UC-IHC	Sesam	●	●			●	●			●	●	●	●
UOU	UOU + FAST v8	●	●			●	●			●	●	●	●
UPC	UPC + FAST	●					○			●	●	●	●
UTokyo	NK-UTWind						○			●	●	●	●
WavEC FAST	FAST v8	●	●			●	●			●	●	●	●
WavEC FF2W	FF2W					●	●			●	●	●	●

For the aerodynamic model, most participants used a blade-element momentum theory-based model, but with varying corrections/attributes. Table 8 indicates whether participants included the influence of a dynamic wake (which models the time lag in the induced velocities created by vorticity being shed from the blades and being

convected downstream) and/or unsteady airfoil aerodynamics (which models flow hysteresis, including unsteady attached flow, trailing-edge flow separation, dynamic stall, and flow reattachment) in some form.

For the hydrodynamic modeling, participants used a potential flow-based solution, a strip-theory solution through Morison's equation, or a combination of the two. The potential-flow models use radiation/diffraction matrices computed from a panel code such as WAMIT, which does not account for viscous effects. Therefore, some participants added the drag term from Morison's equation to their solution, whereas others just added a damping matrix, the latter of which will only capture the damping force and not the potential excitation from viscous loads. Those using a potential-flow model with a damping matrix are indicated by the pink squares in Table 8 under "1st PF." Those using a strip-theory (Morison-only) model are indicated by the pink squares under "ME" in the table. The remainder (and majority) of participants used a potential-flow solution in conjunction with Morison drag, and this approach is indicated by a green square under "ME" as well as a green square under either "1st PF" or "2nd PF," indicating whether a first- or second-order potential-flow solution was used. Additional attributes that contributed to the hydrodynamic load solution include whether the measured wave was used versus a synthetic wave with a JONSWAP spectrum, the inclusion of wave stretching in the wave kinematics treatment, and the calculation of the hydrodynamic forces at the instantaneous position of the structure in the wave field (rather than its initial position). For the moorings, attributes indicated in the table include whether a dynamic mooring line model was used (versus a quasi-static approach), whether hydrodynamic excitation from the waves was included, and if seabed friction was applied to the lines.

5. Calibration

Prior to validation, the numerical models must be calibrated to ensure that they accurately represent the as-built properties of the test specimen. Calibration of properties is needed when there is some uncertainty, and can be related to the environmental conditions (wind/waves) used to excite the structure as well. For this phase of OC5, it was decided that participants would calibrate their models independently. Independent calibration could potentially lead to differences in the simulation results based on differences in calibration approaches, rather than modeling theories. If uncertainty in the model/conditions of the test is small, it will not have a significant impact; however, we do not have enough information in this test campaign to ascertain the levels of uncertainty. As will be discussed later in the paper, this limits our ability to draw conclusions about the reason for differences between the simulations and test measurements. Although model calibration was performed independently, procedures were shared, and so participants largely performed similar calibrations of their models. It is therefore believed that most of the differences between simulated results are caused by the modeling approaches and theories, rather than a direct consequence of calibration.

5.1. Static Equilibrium

The first step to calibrate (and check) the model was to examine the static equilibrium position and loads of the structure floating in still water, as well as the mooring loads for prescribed offset distances. Initial analysis showed that the prescribed properties of the system did not result in a zero-offset static equilibrium. Some participants chose to increase the mass of the platform to achieve the prescribed draft at equilibrium, but this approach reveals that there is some uncertainty in either the prescribed mass, displacement, or mooring pretensions. The CM of the nacelle in the test specimen was adjusted to ensure almost zero pitch offset of the structure without wind, and therefore had some uncertainty associated with it as a result of adjustments that were made.

5.2. Free Decay

The next step was to compare the eigenfrequencies and damping of the system through free-decay tests of the structure for the surge, heave, pitch, and yaw degrees of freedom. Damping was separated into linear and quadratic components. Some participants found it necessary to tune damping coefficients or include additional external damping to the structure to match the behavior of the tests. Also, some participants added extra stiffness to the system in the surge/pitch directions to match the surge/pitch natural frequencies, and a surge preload to match the

static equilibrium of the structure and initial mooring tensions. The need for additional stiffness is assumed to be caused by the influence of the cable bundle on the response of the system. A summary of the test-derived natural frequencies and damping are provided in Table 9.

Table 9. System frequencies and damping (extracted from test data).

Degrees of Freedom	Frequency (Hz)	Period (s)	Damping Coeff. (linear, p) (quadratic, q)
Surge	0.00937	107	0.1095 0.1242
Sway	0.00890	112	0.0795 0.1265
Heave	0.0571	17.5	0.0094 0.2733
Roll	0.0305	32.8	0.0648 0.0625
Pitch	0.0308	32.5	0.0579 0.0686
Yaw	0.0124	80.8	0.1446 0.0165
Tower Bending Fore/Aft (F/A)	0.315	3.18	
Tower Bending Side/Side (S/S)	0.325	3.08	

5.3. Wind-Only Excitation

Wind-only tests were then used to check the turbine/aerodynamic properties of the system. The tuning of the aerodynamic properties was done by the University of Maine, the leader of the DeepCwind project [14]. All participants used these properties with no further calibration. A series of steady wind tests at varying rotor rotational speeds was used to check that these aerodynamic properties resulted in consistent and appropriate thrust and power for the turbine.

A wind profile with a time-varying mean (dynamic wind) was then used to examine the dynamic response of the turbine to wind excitation (average wind speed of 13.05 m/s and rpm of 12.1). The power spectral density (PSD) of the resulting x-direction shear force at the yaw bearing (tower top) is shown in Fig. 4. The prominent peaks in this plot coincide with the pitch natural frequency at about 0.03 Hz, the tower natural frequency at 0.32 Hz, and the blade passing once-per revolution (1P) response at 0.2 Hz, as well as harmonics at 0.4 (2P), 0.6 (3P), and 0.8 Hz (4P). Although it is common to see 1P excitations of the tower from some sort of rotor imbalance and 3P excitations (in three-bladed rotors) due, for example, to the blades passing through the tower influence and turbulence, it is less common to see 2P and 4P excitations. The 1P response is most likely caused by differences in the mass of the individual blades. Numerical investigations of the 2P and 4P excitation show that differences in the aerodynamic properties (such as different pitch settings) or stiffness properties between the individual blades could cause such an excitation (see [13] for further discussion on this topic). The blades of the test turbine were very stiff, and considered rigid for our modeling work, but some participants chose to try to emulate some of the blade harmonic excitation through mass and pitch setting differences.
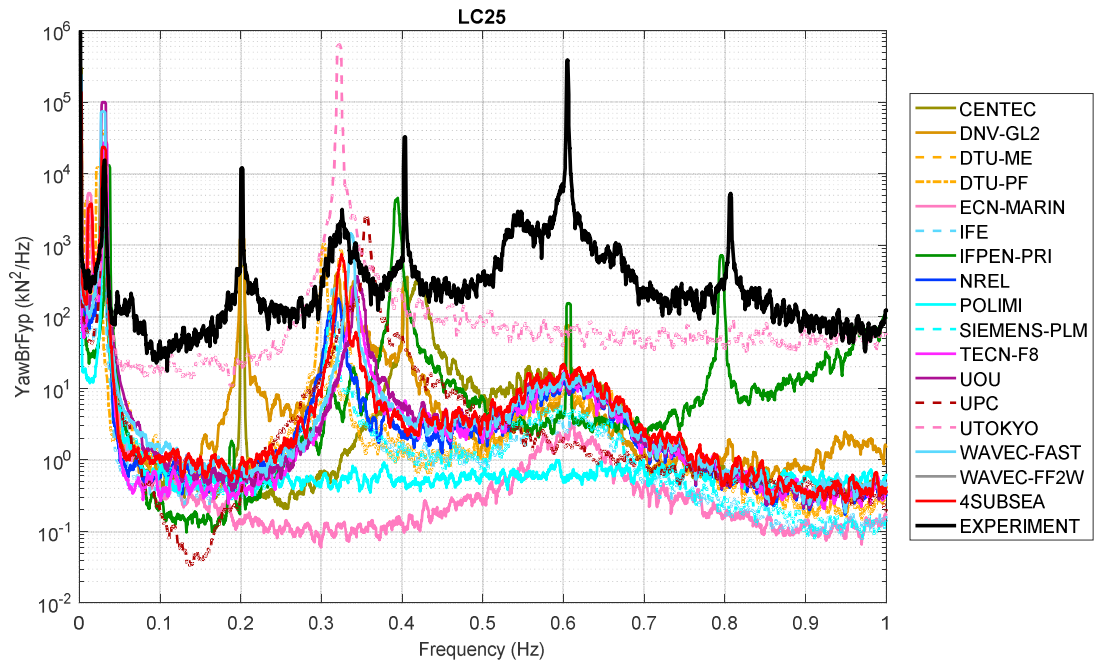
Fig. 4. PSD of tower-top shear force under loading from dynamic wind with a mean wind speed of 13.05 m/s (log scale)

Examination of the yaw bearing shear force (Fig. 4) shows that across a broad band of frequencies, the experiment experiences larger excitation than the participants. The difference could be caused by incorrect representation of the wind excitation or incorrect system properties. Prior to testing, a wind probe was used to assess the spatial variation of the wind in terms of mean value and turbulence. However, there was no time measurement of multiple points in the wind field at the same time, and thus no assessment of the level of spatial coherence. Also, no repeat measurements were provided, so no understanding of the repeatability of the wind conditions is known.

Participants were given a time measurement of the wind field without the turbine present at the location of the hub, and TurbSim [16] was used to generate a full wind field for simulation using International Electrotechnical Commission standard coherence models [17]. Some participants showed that by altering the level of shear, turbulence and coherence, the tower-top loads could be increased. Also, the inclusion of unsteady aerodynamics by participants increased the level of excitation slightly. For the excitation at the tower-bending natural frequency (~0.3 Hz), some participants tuned the damping of this mode to better match the level of excitation seen in the experiment. Additional unmodeled characteristics of the structure itself, such as the influence of the cable bundle, could also create more excitation for the experiment. Without direct access to the test article and facility during the validation process, our ability to draw definitive conclusions about the reason for the load differences is limited.

5.4. Wave-Only Excitation

Two regular wave-only (no wind) tests were then used to examine the wave-structure response of the system (only one is discussed here). A response amplitude operator (RAO) was used to make this comparison, which for regular waves is the ratio between the amplitude of the system motion response to the amplitude of the wave excitation at the wave natural frequency. Fig. 5a shows the RAO for the surge, heave, and pitch DOF (calculated at the SWL) using a wave with a height of 9.41 m and period of 14.3 s. Results are fairly consistent for surge and pitch, but the heave response is significantly underpredicted by some participants. Throughout this validation process, we have seen the following reasons for the underprediction of the heave response:

- Morison-only models need to include calculation of the dynamic pressure on the top and bottom of the base columns

- Viscous-drag calculations need to use the relative velocity between the fluid and structure, and cannot be computed solely from the fluid velocity
- Axial viscous-drag loads on the heave plates are important in capturing the correct heave behavior.

A second area in which differences were seen for this load case was the loads in the mooring lines at the fairlead connection. The magnitude of the RAO for the mooring line response from regular wave excitation (at the wave natural frequency) is shown in Fig. 5b. All three fairlead responses show a difference for those using a quasi-static approach for modeling the mooring line tensions (UTOKYO, WAVEC_FAST, WAVEC_FF2W), as compared to a dynamic model. However, large differences in the motion RAO are not seen for those using a quasi-static mooring model, meaning that a dynamic mooring model is important for accurately representing the loads in the moorings, but does not significantly influence the motion/loads in the remainder of the system. The two regular load cases were used by some participants to set mooring properties (usually the drag coefficient), such that the loads in the moorings matched that of the experiment for the given wave conditions.
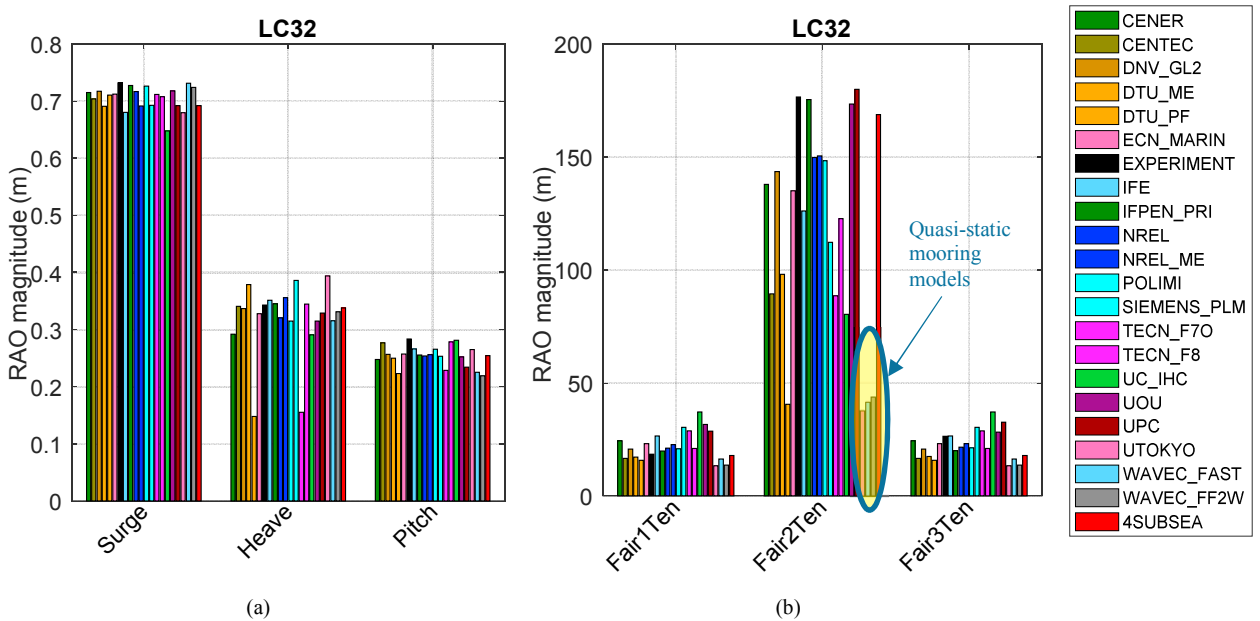
Fig. 5. RAOs for regular wave excitation with a wave height of 9.4 m and period of 14.3 s: (a) the motion RAO, and (b) mooring tension RAO

6. Validation

The objective of this validation project is to assess the ability of the modeling tools to accurately predict the ultimate and fatigue loads of the system (quantities of interest), which is the intended use of the tools. Validation was assessed using a series of irregular wave tests, both with and without wind (see Table 10 for the list of load cases). Although standards prescribe different load cases for assessing ultimate vs. fatigue loads, here we examine both quantities across all validation cases. The ultimate and fatigue loads were computed for the shear forces at the tower top and bottom in the direction of the wind/waves and for the tensions at the fairlead for mooring lines 1 and 2 (see Fig. 2 for the numbering). Ultimate loads were calculated as the highest local peak when the largest 5% of the peaks were eliminated (to eliminate the influence of outliers). The fatigue loads were calculated as the damage equivalent load using Rainflow counting with an equivalent load frequency of 1 Hz, a Whöler exponent of 5, and Goodman correction to account for differences in the mean cycle loads. The ultimate and fatigue loads for both participants and the experiment were calculated using the exact same procedures. Validation is achieved if the simulated ultimate/fatigue loads match within the uncertainty bounds of the measured loads. However, the

uncertainty bounds are not assessed in this exercise, and so, the evaluation in this paper is more of a qualitative one to understand the needs and limitations of the modeling tools.

Table 10. Description of validation test (load) cases – irregular wave excitation with and without wind.

Load Case	Description	rpm	Blade Pitch (deg)	Wave Condition	Wind Condition	Sim. Length (min)
3.3	Operational Wave	0	90	Irregular: H_s = 7.1 m, T_p = 12.1 s, γ=2.2, JONSWAP	N/A	176
3.4	Design Wave	0	90	Irregular: H_s = 10.5 m, T_p = 14.3 s, γ=3.0, JONSWAP	N/A	180
3.5	White Noise Wave	0	90	White noise: H_s = 10.5 m, T_{range} =6-26 s	N/A	180
4.1	Oper. Wave Steady Wind 1	12.1	1.2	Irregular: H_s = 7.1 m, T_p = 12.1 s, γ=2.2, JONSWAP	$V_{hub,x}$= 12.91 , $V_{hub,z}$= -0.343 σ_x = 0.5456, σ_z = 0.2376	180
4.2	Oper. Wave Steady Wind 2	12.1	15.0	Irregular: H_s = 7.1 m, T_p = 12.1 s, γ=2.2, JONSWAP	$V_{hub,x}$ = 21.19, $V_{hub,z}$ = -0.600 σ_x = 0.9630, σ_z = 0.4327	180
4.3	Oper. Wave Dynamic Wind	12.1	1.2	Irregular: H_s = 7.1 m, T_p = 12.1 s, γ=2.2, JONSWAP	NPD spectrum, μ = 13.05	180
4.4	Design Wave Steady Wind 1	12.1	1.2	Irregular: H_s = 10.5 m, T_p = 14.3 s, γ=3.0, JONSWAP	$V_{hub,x}$= 12.91 , $V_{hub,z}$= -0.343 σ_x = 0.5456, σ_z = 0.2376	180
4.5	White N. Wave Steady Wind 1	12.1	1.2	White noise: H_s = 10.5 m, T_{range} = 6-26 s	$V_{hub,x}$= 12.91 , $V_{hub,z}$= -0.343 σ_x = 0.5456, σ_z = 0.2376	180

6.1. Ultimate and Fatigue Loads – All Load Cases

To compare the simulated loads to the measured ones, first the individual participant results were averaged together. In this process, those results that were largely different from other participants were thrown out (those with an absolute difference greater than 50% compared to the experiment). The comparison of the ultimate and fatigue loads for the tower-base shear force is shown in Fig. 6. This plot shows that the participants are (on average) consistently underpredicting the results from the experiment for both the ultimate and fatigue loads, and the fatigue-load differences are generally larger than the ultimate-load differences.
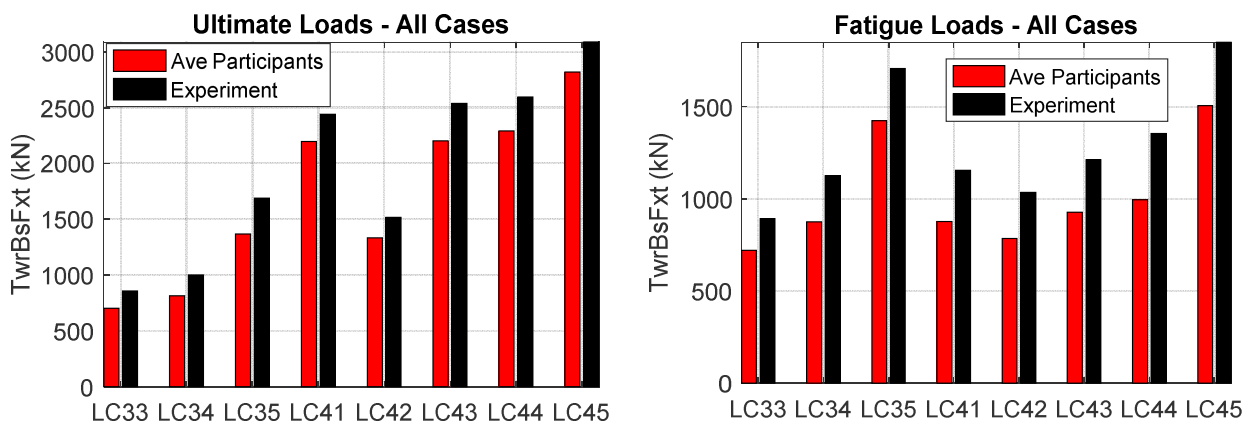

Fig. 6. Comparison of average participant tower-base shear forces to experiment across all validation cases (ultimate and fatigue loads)

The trend of underprediction by the participants is also true for the ultimate and fatigue loads at the tower top and the upwind mooring line (Line 2). Fig. 7 shows the percent difference between the average of the participants and the experiment for each of these measurements, as well as one of the downwind mooring lines (Line 1). The

downwind mooring line is the only one of these measurements that does not show consistent underprediction. The loads in this mooring line are not as influenced by the motion of the turbine, and show very limited variation. When wind is included (LC 4.x), the tower loads are higher than without (LC 3.x), and the fatigue error between the simulation and experiment is generally larger. But, the ultimate tower load errors are smaller when wind is included. The error is also generally larger for the tower-bottom forces than the tower-top forces. Larger waves (LC 3.4 vs. LC 3.3) seem to increase the level of error between the experiment and simulations for the tower ultimate and fatigue loads only slightly. And, the wind speed does not seem to have a significant effect (LC 4.2 vs. LC 4.1). For the mooring line loads, it is difficult to discern any trends in the error based on wind/wave loading scenarios.
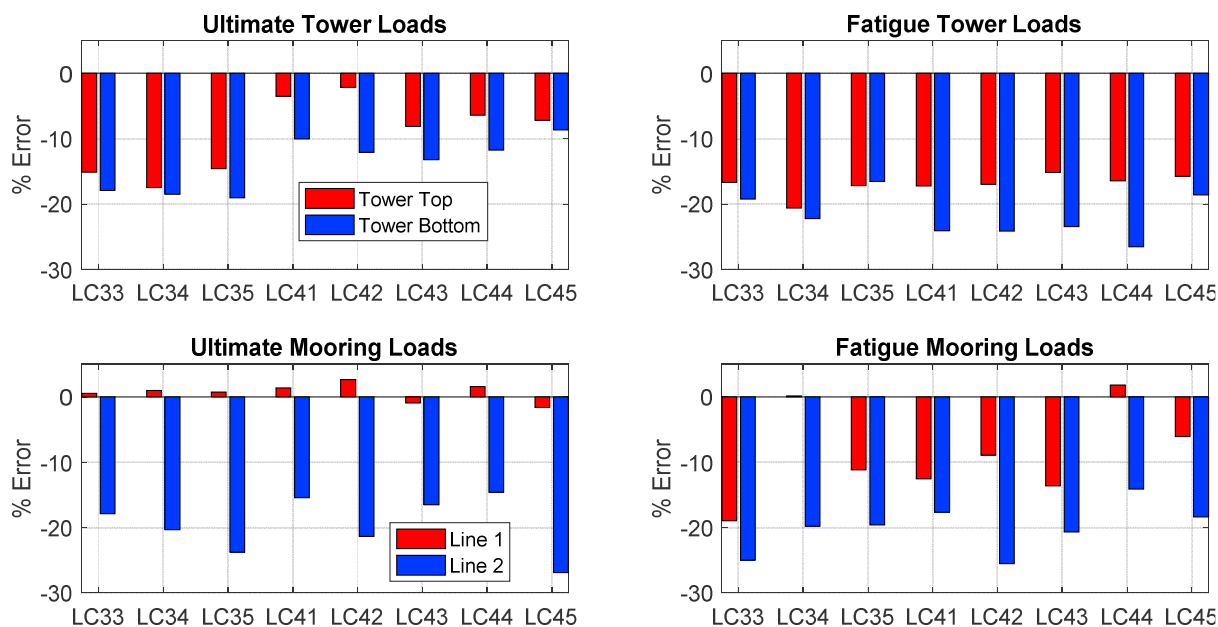
Fig. 7. Percent difference between average of participants and experiment for different load measurements (ultimate and fatigue)

6.2. Tower-Base Load – LC 3.3

Fig. 8 shows the percent difference between individual participants and the experiment for tower-base loads for one of the eight load cases shown above, LC 3.3, which includes only irregular wave excitation with a significant wave height of 7.1 m and peak period of 12.1 s. Colors in the plot are used to delineate between potential-flow (PF)-only models with a drag matrix (red), PF models augmented with Morison drag (blue), and Morison-only models (green). As shown in Fig. 6, most participants are underpredicting the tower-base loads, with the exception of most of the Morison-only models (all except Siemens PLM).

To see what is causing this difference, the PSD of the tower-base loads is examined (see Fig. 9). For this plot, various colors are assigned to the different participants, and results are delineated through dash-dot lines for the PF-plus-drag matrix, solid for the PF-plus-Morison drag, and dashed for the Morison-only models. The figure shows four distinct frequencies in the PSD: the pitch natural frequency at 0.03 Hz, the linear wave excitation at 0.07 and 0.14 Hz, and the tower-bending natural frequency at about 0.32 Hz. The motion of the three-dimensional structure in relation to the waves creates the two distinct peaks from linear wave excitation, with a larger response occurring away from the peak frequency of 0.07 Hz. This plot shows that all tools are underpredicting the response at the pitch natural frequency (see inset zoom of pitch natural frequency in Fig. 9). Those with the largest values (and closest to the experiment) are ones that use second-order PF models. The Morison-only result from IFE is actually the largest, but overestimates the loads in higher frequencies. The pitch natural frequency is outside the linear wave-excitation range, and must be excited by some nonlinear force, such as from second-order PF theory, second-order or higher wave kinematics, wave stretching, or applying the hydrodynamic loads at the instantaneous position of the floater in

the wave field. Most participants are estimating the response in the linear wave-excitation region fairly well, with a small underestimation in the 0.14-Hz region for PF models and some of the Morison-only models, and a small overestimation for the majority of the Morison-only models.
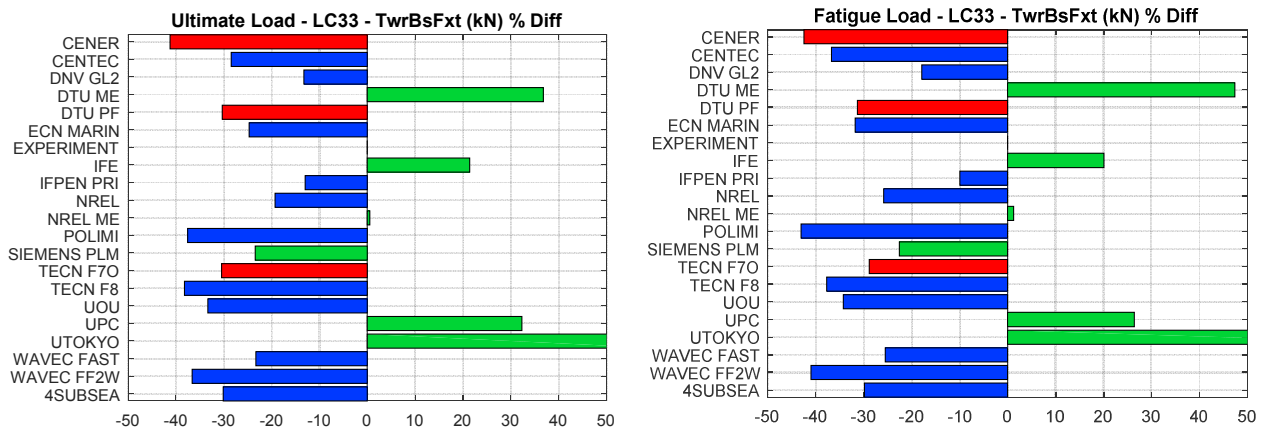

Fig. 8. Percent difference between the participant estimates and experiment for tower-base ultimate and fatigue loads under excitation from an operational-condition wave (some participant values are outside the set scale in the table of -50 to 50%)

Fig. **10** shows the cumulative difference (calculated by summing the integrated PSD difference from low to high frequencies) between the participants and experiment for the tower-base loads. This figure can be used to see at what frequencies the biggest jumps in differences are occurring. For the PF models, the largest jump is at the pitch natural frequency (0.03 Hz). Although the inclusion of nonlinear terms in the wave excitation improves the comparison of the simulation to the experiment, most codes are significantly underpredicting the response at this frequency. The issue could be related to damping. When a drag coefficient of zero is used, a level similar to the experiment can be obtained at the pitch natural frequency. A comparison to a higher-fidelity code, such as a computational fluid dynamics simulation, could enable a better understanding of why the engineering models are not approximating the response at this frequency accurately.

For most of the Morison-only models, the largest differences occur at the tower-bending frequency (0.3 Hz), wherein most of the models go from cumulatively underpredicting the load to overpredicting it. Investigation into the cause of this overexcitation by Morison-only models showed that the excitation at the tower natural frequency is related to the treatment of the added mass. This frequency falls in a region where the diameter over wavelength ratio is greater than 0.2, and thus the added mass coefficient decreases significantly. The Morison-only codes in this investigation allow only one value to be used for the added mass coefficient across all frequencies, and the response therefore is overpredicted in the region where the diameter over wavelength ratio is greater than 0.2, which is around 0.11 and 0.16 Hz for the base and offset columns, respectively. Some participants addressed this issue by low-pass filtering the wave below the tower-bending natural frequency. The associated motion RAOs (derived in LC 3.5) for the linear wave-excitation region are shown in Fig. 11, in which an overestimation of the pitch response is seen for most Morison-only models above about 0.1 Hz.
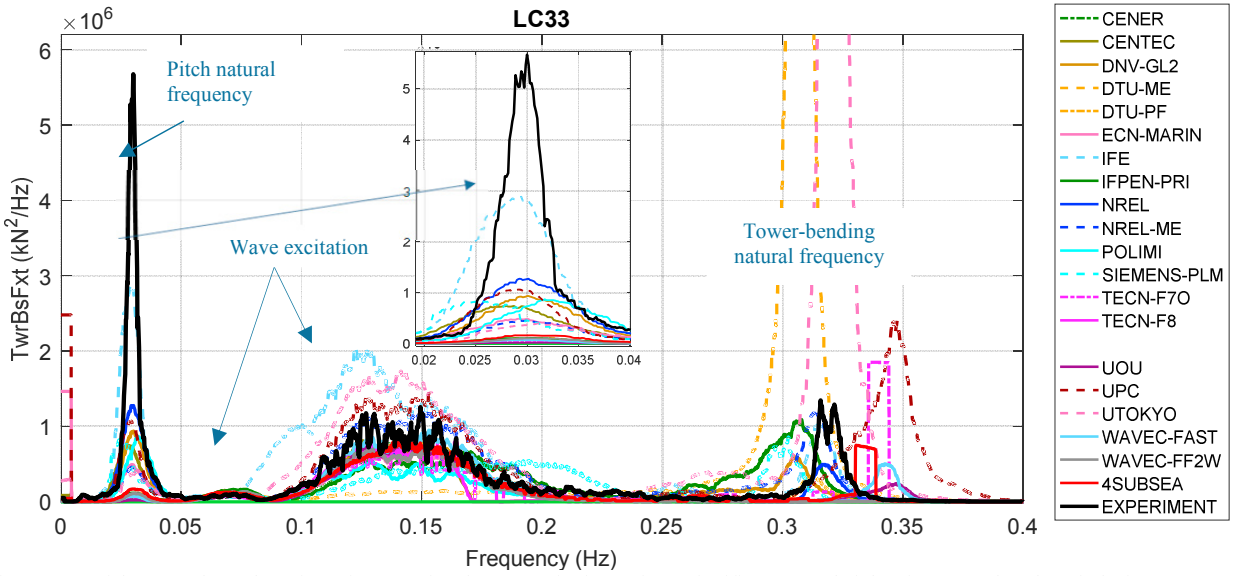
Fig. 9. PSD of the tower-base shear force for operational wave excitation, using a significant wave height of 7.1 m and peak period of 12.1 s
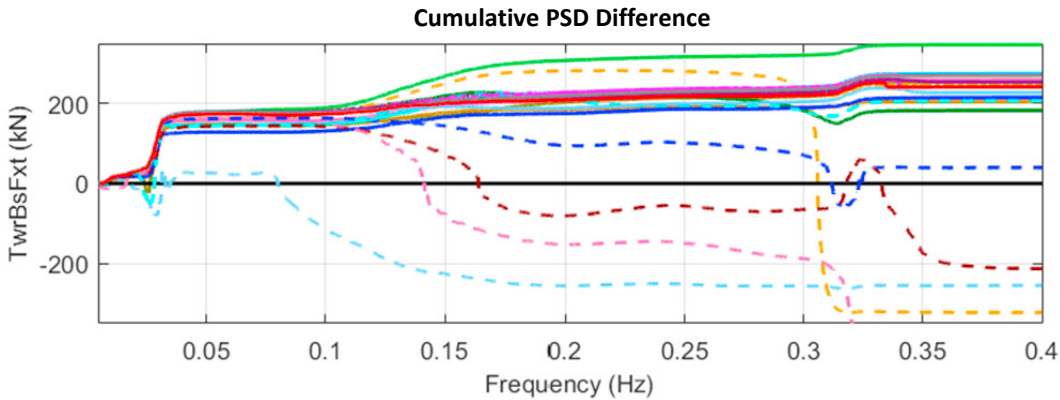

Fig. 10. Cumulative difference in PSD of tower-base shear force for operational wave excitation between the participants and the experiment
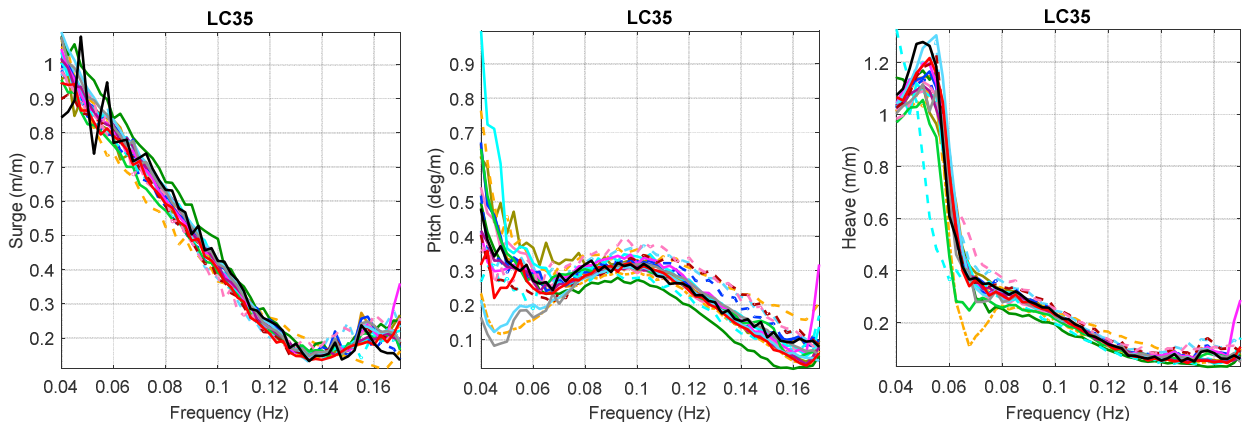

Fig. 11. RAO of motion response based on excitation from a banded white noise wave (LC 3.5)

6.3. Tower-Base Load – LC 4.1

Next, the percent error for the tower-base loads for the same wave condition as LC 3.3, but with wind added, was investigated (LC 4.1). The wind profile is steady wind, with an average speed of 12.91 m/s and a turbulence intensity around 5%, with some drop out near the bottom of the rotor (where the wind-generating fans were unable to blow). The ultimate load errors for this case (see Fig. 12) are very different than without wind, with the majority of all models underpredicting the ultimate load by less than 20%, regardless of modeling approach. The wind has damped out a lot of pitch and tower-bending motion of the structure, which was the source for many of the differences between the simulation and measurements for LC 3.3. However, the fatigue errors are still large, presumably as a result of the influence of the turbulence from the wind on the system response. Here again, we see an overprediction by some of the Morison-only models, but not as many. Examination of the PSD (Fig. 13) shows the diminished responses at the pitch and tower natural frequencies by both the participants and experiment. In the linear wave-excitation region (0.05–0.25 Hz), the experiment shows an increased response with wind compared to without, whereas the simulations do not show as much change. Some additional frequencies are also visible at 0.4 and 0.6 Hz, which are the 2P and 3P rotor frequencies; however, these frequencies do not contribute significantly to either the ultimate or fatigue loads.
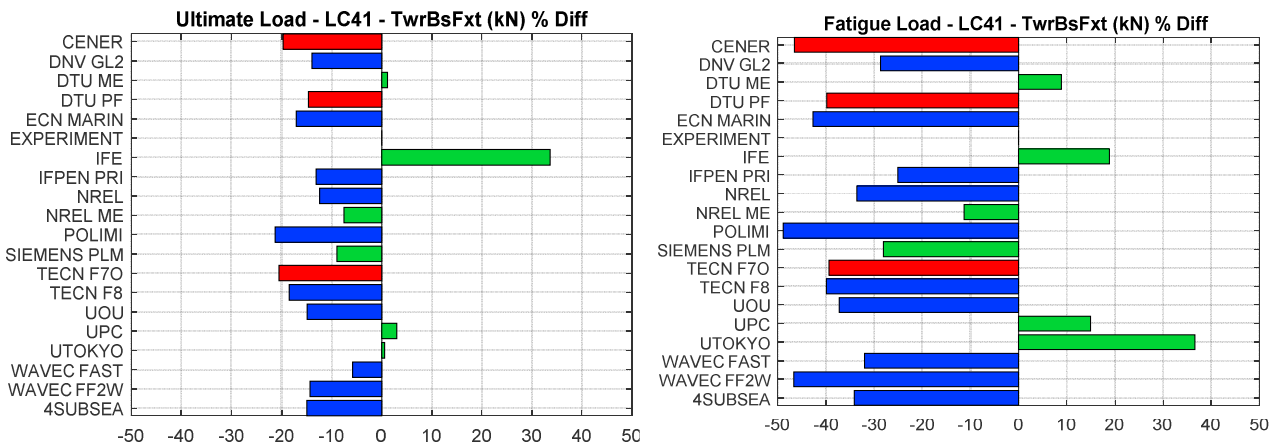

Fig. 12. Percent difference between individual participant estimates of ultimate and fatigue loads for the tower-base shear force under excitation from an operational-condition wave and steady wind at 12.9 m/s (some participant values are outside the set scale in the table of -50 to 50%)
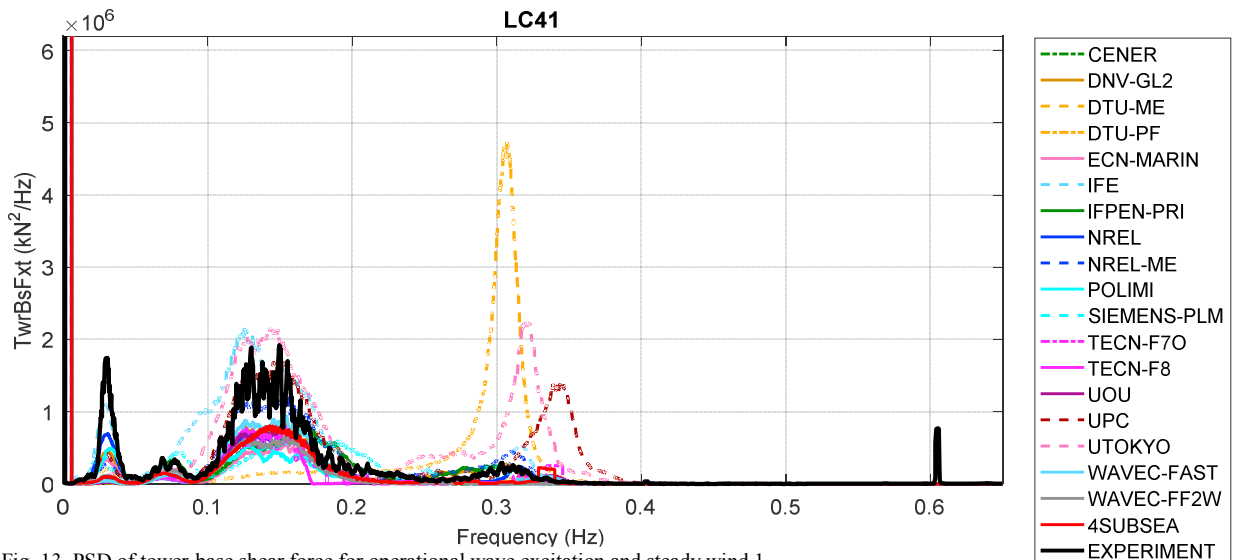

Fig. 13. PSD of tower-base shear force for operational wave excitation and steady wind 1

6.4. Mooring Tension – LC 3.3

Next, we focus on the loads in the mooring lines, specifically we examined the upwind mooring line (Line 2). Ultimate and fatigue load errors for the upwind mooring line with wave-only excitation (LC 3.3) are shown in Fig. 14. For the ultimate load, the participant results are fairly consistent, with all models underpredicting the load with usually less than 30% error. The fatigue loads are also almost all underpredicted, but the errors are greater, especially for those using a quasi-static mooring model, as indicated by the pink color in the plot (blue indicates a dynamic mooring model is being used). As observed in the PSD of the fairlead tension (Fig. 15), participants using a quasi-static mooring model significantly underpredict the mooring loads in the linear wave-excitation region. The underprediction of loads by all participants in the low frequencies is related to underprediction of the surge motion of the system at the surge natural frequency (0.01 Hz).
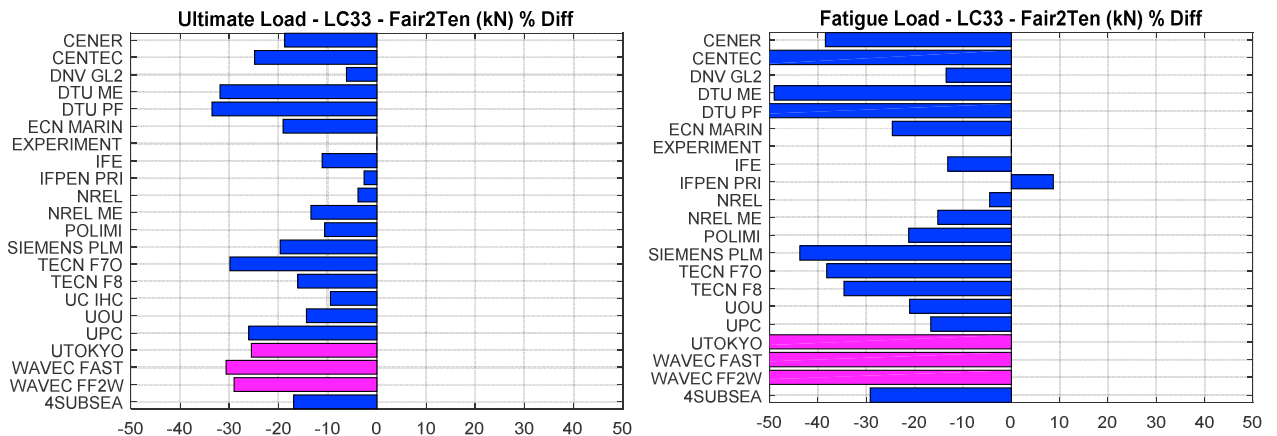

Fig. 14. Percent difference between individual participant estimates of ultimate and fatigue loads for the mooring line 2 tension under excitation from an operational-condition wave (some participant values are outside the set scale in the table of -50 to 50%)
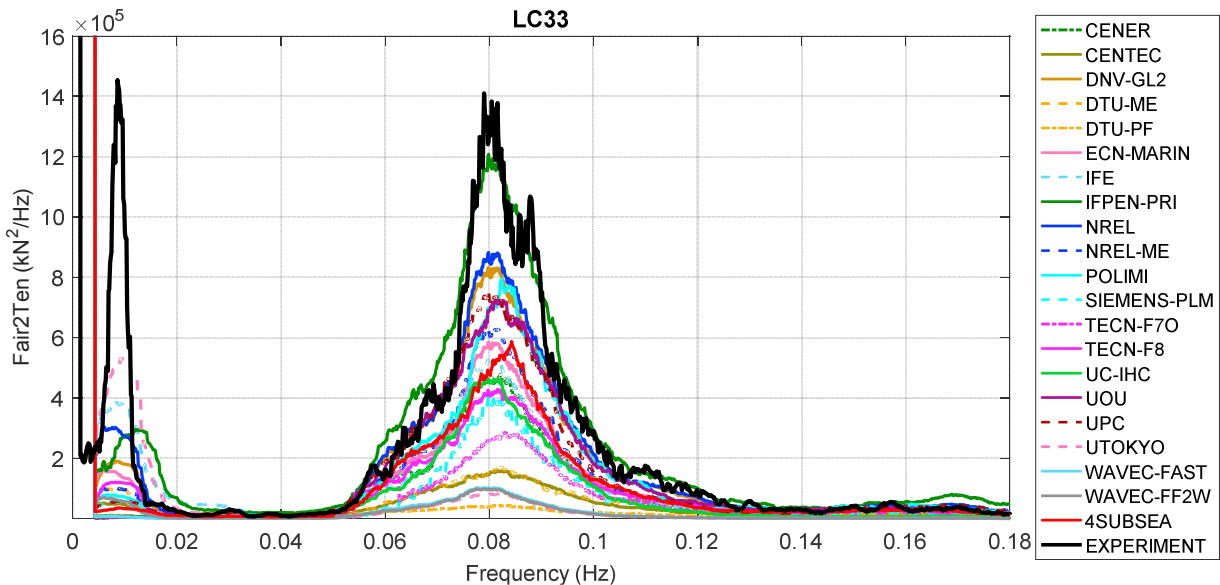

Fig. 15. PSD of mooring line 2 tension for operational wave excitation

6.5. Mooring Tension – LC 3.4 – Slack-Line Events

For some extreme wave events, the mooring lines may go slack and then re-tension themselves. This occurs when the pretension in the lines is not sufficiently large enough to exceed the minimum tension of the lines during extreme events, and is something to be avoided as it can lead to extreme loads in the moorings. Therefore, it is important to be able to predict/model in simulations. For LC 3.4, which has a larger significant wave height (compared to LC 3.3) of 10.5 m, some slack-line events were encountered. Fig. 16a shows the mooring line tension response to three large wave events in succession, as can be seen by a drop in the mooring tension to a value close to zero after the wave passage. Only those participants who are directly importing the measured waves in their simulations are displayed, as otherwise this specific event would not happen at this time. The first thing to notice is that the WavEC solutions, which are the only results shown that use a quasi-static mooring model, do not predict the slack line event, significantly underpredict the mooring loads, and have a phase shift. The other models all predict the drop in the mooring tension, but have various levels of agreement on the large tensions that occur during the extreme wave passage, and as the mooring line rebounds from the loss in tension. Most underpredict the extreme loads in the moorings, with the exception of IFE, IFPEN-PRI, and UPC. IFE, IFPEN-PRI, and DNV GL include excitation of the lines from the waves, which could contribute to the larger loads observed for these models. In Fig. 16b, a probability of exceedance plot is shown for all the local minimum values in the mooring tension response. This plot shows more clearly the differences in mooring tension value distributions, and more evidence of the differences in using a quasi-static mooring model.
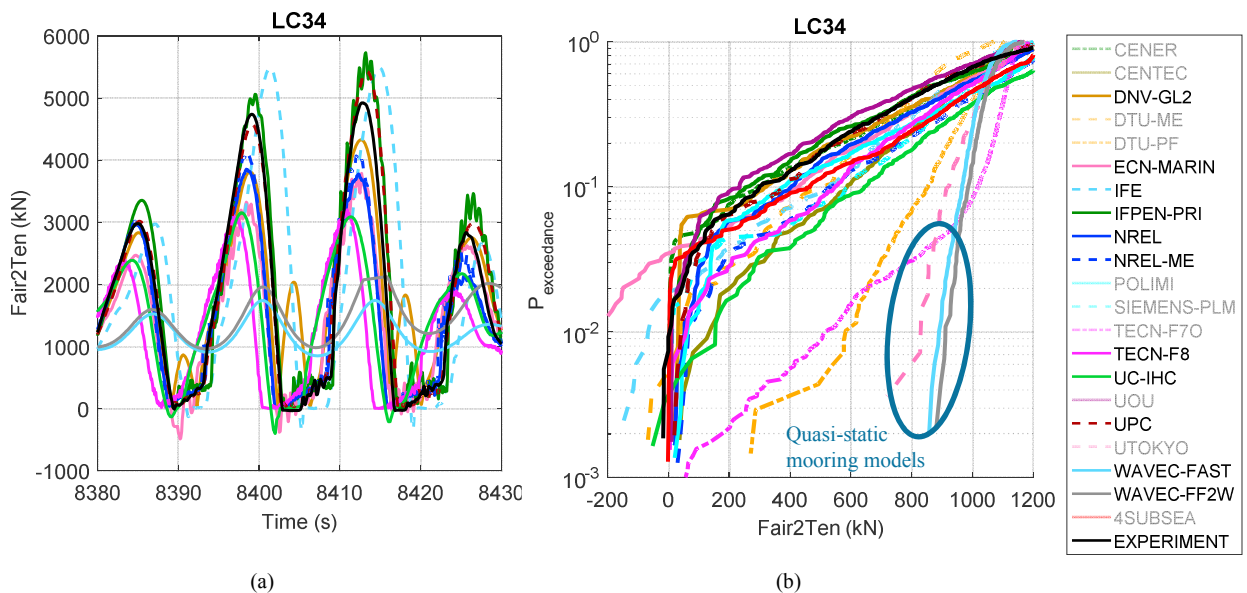

Fig. 16. (a) Time response of line 2 tension during steep wave events, (b) exceedance probability plot of line 2 tension of minimum values

7. Conclusions

The authors of this paper have reviewed the findings from the validation of a model-scale floating semisubmersible within Phase II of the OC5 project. The objective was to validate the ultimate and fatigue loads of the system, which is the intended use of the modeling tools used in this investigation. To claim a successful validation, the predicted loads from the modeling tools should match that of the experimental measurements, within some level of uncertainty. The uncertainty levels in the measurements, however, were difficult to estimate as the testing was done outside of this project, and no uncertainty assessment was performed at the time of testing. This paper therefore focuses only on a general comparison of the results.

The results showed that participants generally underpredicted the ultimate and fatigue loads. The average error across participants for wave-only cases (not including white noise) was about a 10% underprediction of the tower-top ultimate shear load, a 14% underprediction for the tower-base load, and a 20% underprediction of the upwind mooring tension. The fatigue load underprediction was larger: 17% for the tower top, 21% at the tower base, and 21% for the moorings. With wind, the error decreased for the ultimate loads, but stayed about the same or increased for the fatigue. The regions with the largest underprediction of force were the low-frequency responses outside the wave-excitation region, associated with the excitation of the surge and pitch natural frequencies. Because there is no energy excitation from linear waves at these frequencies, the excitations must come from some nonlinear force. The largest simulated responses in this region were observed by those using a second-order potential-flow theory or Morison-only models; but, still, the response level did not meet that of the experimental measurements. This disparity could be caused by the modeling theories not achieving the right level of excitation or by some unmodeled dynamics in the test system. For instance, the cable bundle used for recording measurements from the sensors could impart nonlinear stiffness to the model, which is not represented in the simulations.

The work from this project revealed that some modeling attributes were important in achieving a better match between the simulation and experiment. For the hydrodynamics, nonlinear wave forces are important for accurately capturing the excitation of natural frequencies outside the wave-excitation region, such as the surge, pitch, and tower natural frequencies. Modeling approaches that would produce nonlinear wave forces include second-order potential-flow theory, second-order or higher wave kinematics, wave stretching, and application of the wave-excitation load at the instantaneous position of the body. These attributes will also create a drift force in the system, which may influence the loading in the mooring lines. For moorings, it was observed that having a dynamic (rather than quasi-static) model was important for capturing the ultimate and fatigue loads in the lines, and that the inclusion of hydrodynamic excitation from the waves could create larger loads. There was not much focus given to the aerodynamic models because differences in the hydrodynamic models masked any differences in the aerodynamics. Most participants used a BEM model, but some included the influence of a dynamic wake and unsteady airfoil aerodynamics. Results did show that the use of unsteady airfoil aerodynamics tended to produce more broadband frequency excitation in the system, which helped in matching the experiment. Tower and nacelle drag were shown not to be important to this system because the nacelle and tower tested were fairly small in size compared to a real system.

For the hydrodynamic modeling, participants used either a potential-flow-based solution, Morison's equation, or a hybrid combination of the two. Potential-flow models do not account for viscous effects, and some participants therefore added the drag term of Morison's equation to their solution, whereas others just added a damping matrix to account for viscous effects. It was shown here and within the OC4 project [8] that using a damping matrix can have some limitations. Primarily, to fully represent the viscous drag loading, a full matrix (including nondiagonal terms) must be used, such that coupling between different degrees of freedom is achieved. For those that only used Morison's equation, it was seen that most of these models had larger pitch excitation compared to potential-flow models at higher frequencies. The difference is caused by the limitation of Morison's equation when the diameter to wavelength ratio is greater than 0.2. Above this threshold, the slenderness assumption of Morison's equation is not valid, and diffraction effects that are not modeled by this approach significantly affect the loads. In addition, when using a Morison-only model, to get the proper heave excitation in the system, one must ensure that the dynamic pressure forces are calculated on the ends of the heave plates, as well as axial viscous drag using the relative velocity between the fluid and structure.

As was mentioned many times in this paper, it is difficult to completely determine the reasons for differences between simulations and experimental measurements without an uncertainty assessment of the measurements. The limited amount of data available from this test campaign prohibits a thorough uncertainty assessment, and future test campaigns need to address this limitation [14]. In addition, it would be preferable to do model validation work during the testing so that questions that arise could potentially be addressed through further tests. Furthermore, examination of the OC5 Phase II system with a computational fluid dynamics code, which has a higher-fidelity model of the underlying physics, could help determine if there are some deficiencies in the hydrodynamic models being employed by participants.

8. Acknowledgements

References

[1] IEA Wind Task 31 web page: https://www.ieawind.org/summary_page_31.html.
[2] C. Koch, F. Lemmer, F. Borisade, D. Matha and P.W. Cheng. Validation of INNWIND.EU Scaled Model Tests of a Semisubmersible Floating Wind Turbine. Proceedings of the Twenty-sixth International Ocean and Polar Engineering Conference, 2016.
[3] Bredmose, H. Mariegaard, J., Paulsen, B.T., Jensen, B., Schløer, S., Larsen, T.J., Kim, T. and Hansen, A.M. The Wave Loads project. Final report for the ForskEL 10495 Wave Loads project. DTU Wind Energy Report E-0045, December 2013.
[4] Robertson, A. et al. OC5 Project Phase I: Validation of Hydrodynamic Loading on a Fixed Cylinder, presented at The International Society of Offshore and Polar Engineers Conference, June 2015; NREL Report No. CP-5000-63567.
[5] Robertson, A., et al. OC5 Project Phase Ib: Validation of Hydrodynamic Loading on a Fixed, Flexible Cylinder for Offshore Wind Applications. Energy Procedia, Vol 94, pp. 82-101, 2016.
[6] Robertson, A., Jonkman, J., Vorpahl, F., Popko, W., Qvist, J., Froyd, L., Chen, X., Azcona, J., Uzungoglu, E., Guedes Soares, C., Luan, C., Yutong, H., Pengcheng, F., Yde, A., Larsen, T., Nichols, J., Buils, R., Lei, L., Anders Nygard, T., et al. Offshore Code Comparison Collaboration, Continuation within IEA Wind Task 30: Phase II Results Regarding a Floating Semisubmersible Wind System. Presented at the Ocean, Offshore and Arctic Engineering Conference, June 2014. NREL Report No. CP-5000-61154.
[7] Jonkman, J., Butterfield, S., Musial, W., and Scott, G., Definition of a 5-MW Reference Wind Turbine for Offshore System Development, NREL/TP-500-38060, Golden, CO: National Renewable Energy Laboratory, February 2009.
[8] Goupee, A., Fowler, M., Kimball, R., Helder, J., Ridder, E. Additional Wind/Wave Basin Testing of the DeepCwind Semi-submersible with a Performance-Matched Wind Turbine. Presented at the Ocean, Offshore and Arctic Engineering Conference, June 2014.
[9] De Ridder, E., Otto, W., Zondervan, G., Huijs, F., Vaz, G. Development of a Scaled-Down Floating Wind Turbine for Offshore Basin testing. Proceedings of the ASME 33rd International Conference on Ocean, Offshore, and Arctic Engineering, 2014.
[10] Kimball, R.W., Goupee, A.J., Fowler, M.J., de Ridder, E.-J., and Helder, J. Wind/Wave Basin Verification of a Performance-Matched Scale-Model Wind Turbine on a Floating Offshore Wind Turbine Platform. Proc 33rd ASME Int Conf on Ocean, Offshore and Arctic Eng, San Francisco, California, 9B, 10 pp, 2014.
[11] Helder, J.A. and Pietersma, M. UMaine – DeepCwind/OC4 Semi Floating Wind Turbine Repeat Tests. MARIN Report No. 27005-1-OB, 2013.
[12] Jain, A., Robertson, A.N., Jonkman, J.M., Goupee, A.J., Kimball, R.W., Swift, A.H.P. FAST Code Verification of Scaling Laws for DeepCwind Floating Wind System Tests. 13 pp.; NREL Report No. CP-5000-54221, 2012.
[13] Wendt, F., Robertson, A., Jonkman, J. FAST Model Calibration and Validation of the OC5-DeepCwind Floating Offshore Wind System Against Wave Tank Test Data. To be presented at The International Society of Offshore and Polar Engineers Conference, June 2017.
[14] Robertson, A. et al. Uncertainty Analysis of OC5-DeepCwind Floating Semisubmersible Offshore Wind Test Campaign. To be presented at The International Society of Offshore and Polar Engineers Conference, June 2017.
[15] Goupee, A. J., Kimball, R. W., de Ridder, E., Helder, J., Robertson, A. N., Jonkman, J. M. A Calibrated Blade-Element/Momentum Theory Aerodynamic Model of the MARIN Stock Wind Turbine. Presented at the Ocean, Offshore and Arctic Engineering Conference, June 2015.
[16] Jonkman, B. and Buhl, M. TurbSim User's Guide. NREL Report No. TP-500-36970.
[17] IEC 61400–1 ed. 2, Wind Turbine Generator Systems – Part 1: Safety Requirements, International Electrotechnical Commission (IEC), 1999.